Original Research Paper

Combination therapy to overcome ferroptosis resistance by biomimetic self-assembly nano-prodrug

Yong Huang [b,c,1], *Yi Lin* [a,d,1], *Bowen Li* [b,*], *Fu Zhang* [b], *Chenyue Zhan* [b], *Xin Xie* [c], *Zhuo Yao* [b], *Chongzhi Wu* [b], *Yuan Ping* [b,*], *Jianliang Shen* [a,d,*]

[a] *School of Ophthalmology & Optometry, School of Biomedical Engineering, Wenzhou Medical University, Wenzhou 325035, China*
[b] *College of Pharmaceutical Sciences, Zhejiang University, Hangzhou 310058, China*
[c] *Guangdong Provincial Key Laboratory of Research and Development of Natural Drugs, and School of Pharmacy, Guangdong Medical University, Dongguan 523808, China*
[d] *Wenzhou Institute, University of Chinese Academy of Sciences, Wenzhou 325000, China*

ARTICLE INFO

ABSTRACT

Ferroptosis has emerged as a potent form of no-apoptotic cell death that offers a promising alternative to avoid the chemoresistance of apoptotic pathways and serves as a vulnerability of cancer. Herein, we have constructed a biomimetic self-assembly nano-prodrug system that enables the co-delivery of gefitinib (Gefi), ferrocene (Fc) and dihydroartemisinin (DHA) for the combined therapy of both ferroptosis and apoptosis. In the tumor microenvironment, this nano-prodrug is able to disassemble and trigger drug release under high levels of GSH. Interestingly, the released DHA can downregulate GPX4 level for the enhancement of intracellular ferroptosis from Fc, further executing tumor cell death with concomitant chemotherapy by Gefi. More importantly, this nano-prodrug provides highly homologous targeting ability by coating related cell membranes and exhibits outstanding inhibition of tumor growth and metastasis, as well as no noticeable side-effects during treatments. This simple small molecular self-assembled nano-prodrug provides a new reasonably designed modality for ferroptosis-combined chemotherapy.

* Corresponding authors.
E-mail addresses: bowen_86@nus.edu.sg (B. Li), pingy@zju.edu.cn (Y. Ping), shenjl@wiucas.ac.cn (J. Shen).
[1] The authors contributed equally to this work.
Peer review under responsibility of Shenyang Pharmaceutical University.

1. Introduction

Ferroptosis, as an emerging non-apoptotic mode of cell death, is dependent on the oxidation of iron and mediated by lipid peroxidations (LPOs), which can induce tumor cell death and reduce chemo-resistance from traditional apoptotic pathways [1–4]. As an iron-dependent cell death form, ferroptosis is closely related to the presence of bioavailable ferrous iron (Fe^{2+}), which participates in the Fenton reaction with hydrogen peroxide (H_2O_2), resulting in the production of virulent ·OH [5]. Therefore, the *in vivo* delivery of Fe^{2+} plays an important role in triggering tumor-specific ferroptosis, but it is often restricted by the nature characteristics of oxidability, instability in blood circulations, and low tumor selectivity. To overcome these obstacles, many works focus on the delivery of Fe^{2+} source in nanomedicine has begun in recent years, while most studies still rely on the different nanocarriers to load Fe^{2+} [6–12]. However, it still faces some problems in the loading of Fe^{2+} due to the oxidation of Fe^{2+} during transportation with poor drug loading efficiency. Therefore, avoiding oxidation and improving drug loading efficiency have become urgent problems to be solved in ferroptosis nanomedicine. Ferrocene (Fc), as a metal-organic complex, is composed of two cyclopentadienes and Fe^{2+}, which displays excellent chemical stability, hydrophobicity and non-toxicity, can serve as an effective Fe^{2+} source in the treatment of ferroptosis nanomedicine [13–16].

Recently, solid evidence revealed that some antioxidant signal pathways can effectively inhibit the overexpression of lipid peroxides (LPOs), further induce ferroptosis resistance to against cell death [17–20]. Glutathione peroxidase 4 (GPX4) is a glutathione (GSH) and selenium-dependent glutathione peroxidase that detoxifies LPOs formation during oxidative stress, which plays an important role in the antioxidant signal pathway (system x_c^--GSH-GPX4) [21–23]. The development of GPX4 inhibitors in system x_c^--GSH-GPX4 can downregulate the ferroptosis resistance and enhance the therapeutic effect [24]. Recent studies have shown that dihydroartemisinin (DHA) as a derivative of the natural compound artemisinin, not only widely used in the treatment of malaria, but also used as an inhibitor of GPX4 for the inhibition of ferroptosis resistance by system x_c^--GSH-GPX4 [25–31]. Therefore, using the drug co-delivery strategy of Fc and DHA to achieve the combination therapy may provide a new approach to solving the problem of the poor therapeutic efficacy in ferroptosis. The small molecular self-assembly nano-prodrug mediated by disulfide bond has been explored to integrate the advantages of combination therapy and prodrug, which is able to achieve the co-delivery of different drugs with high drug loading and good tumor selectivity [15,32-34]. In this nano-prodrugs, the disulfide bond is crucial for the mediation of self-assembly behavior and also acts as a GSH-responsive bond to trigger drug release. In addition, this self-assembly behavior can also load some drug molecules by hydrophobic and hydrogen-bond interactions, which provide an "all-in-one" strategy of combination therapy for further enhanced therapeutic effects [35–38].

Herein, we developed a biomimetic nano-prodrug system for the co-delivery of ferroptosis drugs (Fc and DHA) and anti-cancer drugs (gefitinib, Gefi) for ferroptosis-combined chemotherapy. As shown in Scheme 1, the disulfide linkage of Fc and Gefi in small molecular prodrug endowed well self-assembly behavior to form a stable nanoparticle (GSSF), following by adding DHA with GSSH in aqueous solution, a three-component nano-prodrug DHA@GSSF could further obtain. In the tumor microenvironment (TME), Fc could trigger the Fenton reaction and induce ferroptosis, and the disassembly behavior of DHA@GSSF could be triggered by high level of GSH, resulting in tumor-selectivity of drug release. The introduction of related cancer cell membrane onto DHA@GSSF led to an effective tumor-targeted delivery and stability in blood circulations, resulting in good accumulation of biomimetic nano-prodrug (CM-DHA@GSSF) in tumor site. Eventually, the *in vivo* inhibition of tumor growth and metastasis, and biosafety were investigated on different mice models, which provided a simple and high-efficiency ferroptosis-combined chemotherapy.

2. Materials and methods

2.1. Materials and instruments

Ferrocenecarboxylic acid, 2,2'-dithiodiethanol, oxalyl chloride, N, N-diisopropylethylamine (DIPEA), gefitinib, triphosgene, 4-dimethylaminopyridine (DMAP), methylene blue (MB), indocyanine green (ICG), anhydrous sodium sulfate, ethyl acetate, methanol and dichloromethane (DCM) were purchased from Aladdin Reagents. BODIPY^TM 581/591 C11, RIPA lysis and extraction buffer and BCA protein assay kit were purchased from Thermo Fisher Scientific. D-Luciferin potassium salt, DAPI, ROS assay kit, CCK8 kit, Annexin V-FITC apoptosis detection kit, and Cell viability/cytotoxicity assay kit were provided by Beyotime. All antibodies were obtained from Proteintech. SDS-PAGE gel kit and loading buffer were provided by Solarbio Science & Technology Co. Ltd.

Nuclear magnetic resonance (NMR) spectra were recorded on Bruker Avance 500 MHz NMR spectrometer. High resolution mass spectrometry (HR-MS) was measured on the Agilent 6224 Accurate-Mass TOF LC/MS system. The absorbance spectra were obtained from a UV–Vis spectrophotometer (Hitachi U-3010). Transmission electron microscopy (TEM) images were performed on Hitachi HT7700. The DLS and zeta potentials of nanoparticles were determined on Malvern Nano-ZS90. The fluorescence images in cell were performed on fluorescence microscope (Olympus IX71). The CLSM images in cell were obtained on Leica TCS SP8. Flow cytometry was performed on BD Accuri C6 flow cytometer. The fluorescence images *in vivo* and *ex vivo* were performed on a BLT AniView multimodal imaging system.

2.2. Synthesis of 2-((2-hydroxyethyl)disulfaneyl)ethyl ferrocenecarboxylate

Under nitrogen atmosphere, Ferrocenecarboxylic acid (2 mmol, 460 mg) dissolved in DCM (10 ml) was subjected to dropwise addition of Oxalyl chloride (10 mmol, 850 µl), and the mixture was stirred at room temperature for 3 h. After stirring, the solvent was evaporated, and the residue was
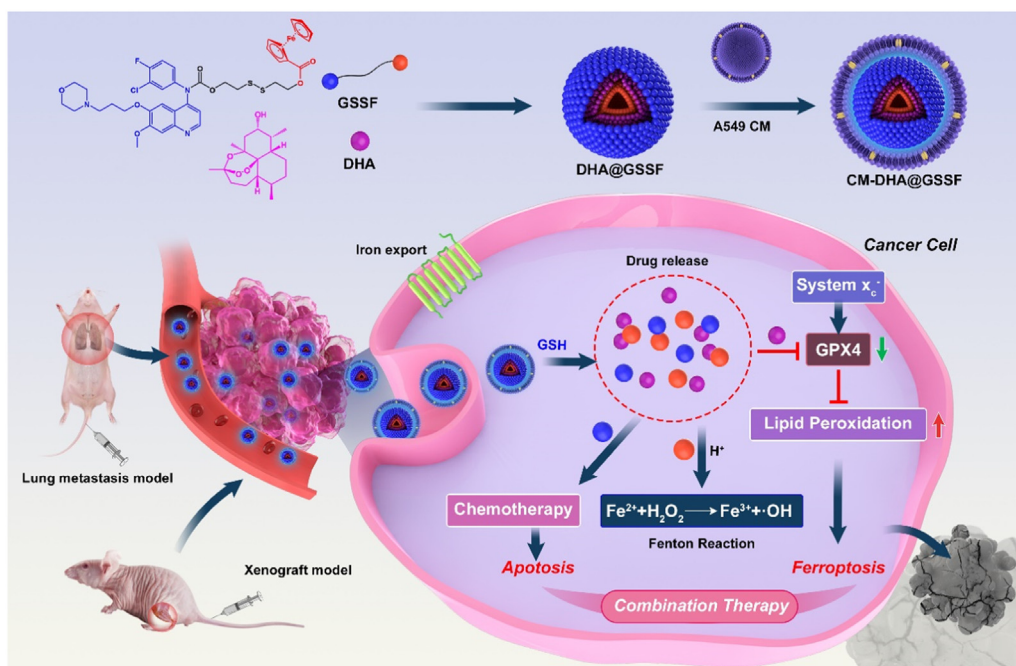
Scheme 1 – Schematic illustration the fabrication and the co-delivery of ferrocene, gefitinib and DHA from biomimetic nano-prodrug CM-DHA@GSSF and promote the more efficient ferroptosis to execute tumor cell death with concomitant chemotherapy.

dissolved in DCM (5 ml). The solution was then added into the mixture of 2,2′-dithiodiethanol (6 mmol, 924 mg) and DIPEA (4 mmol, 900 µl) dissolved in DCM (10 ml) dropwise. The reaction was stirred for 4 h at room temperature. Then, the resulting mixture was extracted, washed and dried. Subsequently, the product was purified through column chromatography (DCM: MeOH=100:1, v/v) to obtain 2-((2-hydroxyethyl)disulfaneyl)ethyl ferrocenecarboxylate as a deep brown solid (388 mg, 53%). ^{1}H NMR (500 MHz, DMSO–d6) δ 4.93 (t, J = 5.5 Hz, 1H), 4.76 (t, J = 1.9 Hz, 2H), 4.51 – 4.50 (m, 2H), 4.40 (t, J = 6.2 Hz, 2H), 4.25 (s, 5H), 3.66 (td, J = 6.4, 5.4 Hz, 2H), 3.07 (t, J = 6.2 Hz, 2H), 2.86 (t, J = 6.5 Hz, 2H).

2.3. Synthesis of 2-((2-(((3-chloro-4-fluorophenyl)(7-methoxy-6-(3-morpholinopropoxy)uinoline-4-yl)carbamoyl)oxy)ethyl)disulfaneyl)ethyl ferrocenecarboxylate

Gefitinib (0.89 mmol, 398 mg) and DMAP (2.67 mg, 410 mg) were dissolved in DCM (10 ml), to which triphosgene (0.36 mmol, 105 mg) dissolved in DCM (2 ml) was gradually added dropwise. After stirring for 1.5 h, the white suspension mixture transformed into a dark red solution. Subsequently, the compound 2-((2-hydroxyethyl)disulfaneyl)ethyl ferro-cenecarboxylate (0.89 mmol, 326 mg) dissolved in DCM (3 ml) was added dropwise to the solution and stirred overnight at room temperature. The resulting mixture was extracted, washed and dried. The product was purified through column chromatography (DCM: MeOH=20:1, v/v) to obtain 2-((2-(((3-chloro-4-fluorophenyl)(7-methoxy-6-(3-morpholinopropoxy)uinoline-4-yl)carbamoyl)oxy)ethyl)

disulfaneyl)ethyl ferrocenecarboxylate as a reddish brown solid (514 mg, 69%). ^{1}H NMR (500 MHz, Chloroform-d) δ 9.05 (s, 1H), 7.48 (dd, J = 6.4, 2.7 Hz, 1H), 7.36 (s, 1H), 7.27 – 7.24 (m, 2H), 7.12 (t, J = 8.6 Hz, 1H), 7.09 (s, 1H), 4.78 (t, J = 1.9 Hz, 2H), 4.48 (t, J = 6.3 Hz, 2H), 4.41 – 4.40 (m, 2H), 4.38 (t, J = 6.6 Hz, 2H), 4.19 (s, 5H), 4.14 (t, J = 6.3 Hz, 2H), 4.04 (s, 3H), 3.75 (s, 4H), 2.92 (t, J = 6.4 Hz, 2H), 2.88 (t, J = 6.3 Hz, 2H), 2.61 (m, 2H), 2.53 (m, 4H), 2.15 – 2.08 (m, 2H). ^{13}C NMR (126 MHz, Chloroform-d) δ 171.57, 157.72, 156.91, 155.65, 153.82, 153.57, 151.13, 150.84, 136.94, 128.51, 126.12, 121.53, 117.67, 116.97, 116.80, 107.07, 101.79, 71.51, 70.54, 70.18, 69.86, 67.42, 66.73, 64.37, 61.81, 56.52, 55.32, 53.60, 37.46, 37.14, 25.71. HR-MS (ESI): calcd for $C_{39}H_{42}ClFFeN_3O_7S_2^+$ ([M+H]$^+$) 838.1481, found: 838.1484.

2.4. Fabrication of nano-prodrug DHA@GSSF

The nanoparticle DHA@GSSF was prepared by a simple nano-precipitation approach. During the procedure, a solution of GSSF (4 mg) and DHA (2 mg, as loading drug) in DMSO (200 µl) was gradually introduced into 10 ml deionized water, and the mixture was stirred vigorously at room temperature for 12 h. The obtained dispersion was then subjected to dialysis against distilled water via a dialysis bag (MWCO 1000 Da) for 24 h to eliminate the organic solvent and free DHA from the DHA@GSSF nanoparticles.

The DHA loading in DHA@GSSF was performed by using the ultraviolet absorption method [30]. Briefly, a solution of DHA@GSSF (1 mg) in DMSO (2 ml) was incubated with 0.2% NaOH for 30 min at 50 ℃, and the solution was measured using UV–vis spectrometer at 290 nm. Then, the drug loading ratio (DLR) of DHA was calculated as 30.6% using

the equation:

$$DLR\ (\%) = Loaded\ DHA's\ mass/DHA@GSSF's\ mass \times 100\%$$

Similarly, we changed the loading drug as blank or ICG to obtain GSSF NPs and ICG@GSSF nanoparticles.

2.5.   Preparation of the biomimetic nano-prodrug CM-DHA@GSSF

To prepare the biomimetic nano-prodrug CM-DHA@GSSF, the coating method of cancer cell membrane was used [10]. In brief, the A549 cells were harvested and washed with PBS, after which the cells were mixed with a solution of EDTA-free protease inhibitor in the lysing buffer and mechanically disrupted with ultrasonic apparatus at 200 W for 5 min, following centrifuged at 3200 g for 10 min. The resulting supernatant was collected and centrifuged at 20,000 g for 20 min, after which the supernatant was centrifuged again at 100,000 g for 30 min to obtain the membrane. To fabricate the cell-membrane coated nanoparticles, the A549 membranes were mixed with DHA@GSSF or ICG@GSSF solution, and then the mixture was extruded via Avanti mini-extruder with polycarbonate membrane (250 nm) for 10 times using to gain the biomimetic nano-prodrug CM-DHA@GSSF and CM-ICG@GSSF.

2.6.   Drug release experiment in vitro

The release assays of DHA, gefitinib and Fc from CM-DHA@GSSF were carried out using a dialysis method. The sealed dialysis bag (MWCO 3500 Da) containing 5 ml CM-DHA@GSSF solution (2 mg/ml) was placed in 30 ml PBS solution with varying concentrations of GSH (0, 0.05, 0.1, 1 and 10 mM). At specific time points, the dialysate solution was taken out and the release behavior of DHA was analyzed by UV–vis absorbance spectra, while that of gefitinib and Fc were analyzed using HPLC.

2.7.   Assessment of ·OH generation

A colorimetric method based on the degradation of MB was used to evaluate the ·OH generation of various samples. The various formulations were incubated with H_2O_2 (1 mM), GSH (10 mM) and MB (20 μM) in different pH value's solution (pH 7.4, 6.8 and 5.5) at 37 °C for 1 h. The degradation percentage of MB was calculated by monitoring the UV–vis absorbance of MB at 664 nm at reasonable time points.

2.8.   Cell culture

All cells (A549, A549-luci, HepG2, HeLa, LO2, and 293T) were cultured in RPMI 1640 or DMEM medium supplemented with 10% (v/v) fetal bovine serum and penicillin-streptomycin (1×), and placed in an incubator at 37 °C with 5% CO_2.

2.9.   Evaluation of intracellular ROS

For monitoring the ROS in the cells after treated with different formulations, the commercial ROS kit was used.

All kinds of the experiments' cells were first planted in 12-well plates and reached about 70% confluence, respectively. The cells were then treated with CM-DHA@GSSF for 6 h, followed by the addition of DCFH-DA (20 μM) probe from the commercial kit and incubated for 30 min. After washing with PBS thrice, the cells were observed under a fluorescence microscope. Additionally, the ROS generation capacity of various formulations treatments in A549 cells was also evaluated with the similar protocol.

2.10.   Cell viability assays

For exploring the cytotoxicity of various formulation's nano-prodrugs, A549 cells and the other cells (HepG2, HeLa, LO2, and 293T) were first planted in 96-well plates and then incubated until they reached about 80% confluence. Then, different concentrations (from 0 to 500 μg/ml) of PBS, Fc, DHA, Gefi, GSSF NPs, DHA@GSSF and CM-DHA@GSSF were respectively added into the well plates and incubated for 48 h. The CCK8 kit was employed to quantitatively analyze the cell viability. The cell viability experiments of nano-prodrug in different types of cells were also determined by using CCK8 kit, with a similar protocol. To clarify the synergistic effect of the DHA and GSSF, the A549 cells were treated with different concentrations of DHA or GSSF alone, or incubation with the two drugs under different ratios. The cell viability experiments of the treated cells were also determined by using a CCK8 kit.

2.11.   Live/dead cell staining

For further evaluating the cytotoxicity of various formulation's nano-prodrugs, A549 cells were first planted in 24-well plates and then incubated until they reached about 80% confluence. They were then treated with PBS, Fc, DHA, Gefi, GSSF NPs, DHA@GSSF and CM-DHA@GSSF for 24 h. Subsequently, the treated cells were measured using Calcein AM/PI kit and imaging via a fluorescence microscope.

2.12.   Western blot assays

The western blot assay was conducted to confirm the presence of cell membrane on nano-prodrug. The cell membrane protein was extracted according to the protocol of commercial kit from Beyotime. The extracted membrane proteins were subjected to separate through gel electrophoresis assay, and the gel was stained with Coomassie blue solution for 30 min. After that, the gel was washed with ddH₂O five times, each for 10 min.

Similarly, western blot was also employed to evaluate the level of GPX4. A549 cells were cultured with different formulation's nano-prodrugs. The treated cells were washed and harvested for protein extraction using RIPA lysate, and the BCA protein assay kit was used to quantify total protein. The extracted proteins were separated through SDS-polyacrylamide gel electrophoresis assay and transferred onto polyvinylidene fluoride (PVDF) membranes. Then, the PVDF membranes were blocked with 5% nonfat milk and incubated overnight at 4 °C with the primary antibody against GPX4 (1:1,000). The tumor dissected tissue was sheared into fine fragments. Then the RIPA lysate was added and mixed at

a ratio of 250 µl lysate per 20 mg tissue, and homogenized with a glass homogenizer until fully cracked. After full lysis, the cells were centrifuged at 14,000 g for 5 min, and the supernatant was removed for subsequent western blot operations. The WB process of GPX4 expression in tumor tissues is similar to that of the cells according to the protocol. After incubating with the peroxidase-conjugated antibody for 1 h, blots were visualized by enhanced chemiluminescence detection.

2.13.   Lipid peroxidation evaluation

To evaluation of the intracellular lipid peroxidation levels of treated with different formulations, the BODIPY^{TM} 581/591 C11 fluorescence probe was used. A549 cells were treated with nano-prodrug and other formulations (PBS, Fc, DHA, Gefi, GSSF, DHA@GSSF, and CM-DHA@GSSF) at the same concentrations of Fc (9.5 µg/ml) and DHA (15.3 µg/ml) for 12 h. After that, the media was substituted with fresh medium containing BODIPY probe (5 µM) for 30 min. Finally, the excess probe was discarded, and the cells were cleaned with PBS before being observed by confocal microscopy.

2.14.   Apoptosis analysis by flow cytometry

To conduct apoptosis analysis, A549 cells with 80%−90% confluence were cultured with fresh medium, or the fresh medium containing the 7 groups of different formulations (PBS, Fc, DHA, Gefi, GSSF NPs, DHA@GSSF and CM-DHA@GSSF), then cells were incubated for further 24 h. After that, the cells washed with PBS, and harvested after trypsinization. The collected cells were centrifugated and resuspended in PBS buffer to remove medium and trypsin. Then, the cells were incubated with binding buffer (400 µl) containing Annexin V-FITC and PI. Flow cytometry analyses were subsequently carried out on a BD Accuri C6 flow cytometer.

2.15.   In vivo antitumor therapy on A549-subcutaneous xenograft model

The animal experiments were conducted according to guidelines of the Laboratory Animals Welfare and Ethics Committee of Zhejiang University. The BALB/c mice were cared for in a sterile condition at the Laboratory in Animals Centre, Zhejiang University.

Before study in vivo, we evaluated the hemolysis of different formulations' nano-prodrugs. We first got the blood from BALB/c mice and extracted the erythrocyte through centrifugation. After incubation of erythrocyte and different formulations for 1 h at 37 °C, the samples were centrifuged to obtain the supernatant, and followed to measure the absorption value.

Pharmacokinetic in vivo: for the pharmacokinetic analysis, the tumor-bearing mice ($n = 3$) were intravenously injected with different samples (DHA, DHA@GSSF and CM-DHA@GSSF) at an equivalent dose of DHA (3.06 mg/kg). After injection, the venous blood samples of mice were collected at different times (5 min, 30 min, 1, 2, 4, 8, 12 and 24 h) and centrifuged to obtain plasma, and the concentration of DHA was measured by UV–Vis absorbance spectra.

To establish an A549-subcutaneous xenograft model, A549 cells (1×10^6) were subcutaneously injected into the right forelimb of each mouse. Once the tumor volume reached about 100 mm^3 (Tumor volume (V) was estimated: $V = \text{Length} \times \text{Width}^2 /2$), the tumor-bearing mice were randomly divided into 4 groups (PBS, ICG, ICG@GSSF and CM-ICG@GSSF) to acquire fluorescent imaging of the mice. The mice were intravenously injected with different formulations at the same dose of ICG (5 mg/kg). After injection for different time (0 h, 1 h, 4 h, 12 h, 24 h, 36 h and 48 h), fluorescence imaging was performed on an in vivo fluorescence imaging system. Then, the mice were sacrificed to collect the main organs and tumors for ex vivo fluorescent imaging.

As the same time, the tumor-bearing mice were treated intravenously with various samples (PBS, Fc, DHA, Gefi, GSSF NPs, DHA@GSSF and CM-DHA@GSSF as 7 group, at an equivalent dose DHA (3.06 mg/kg) and GSSF (16.94 mg/kg) for each mouse) every 2 d for five times. During the period of therapy, the body weight and tumor volume were both recorded every 2 d. The H&E staining analysis for the main organs and tumors collected from the mice were performed after 30-d treatment. The survival rates of every group were also calculated until Day 54.

2.16.   In vivo antitumor therapy on A549 lung metastasis model

A549-luci cells (1×10^6) were first injected into BALB/c nude mice through tail vein to establish A549 lung metastasis model. Similarly, the mice were administered intravenously with various samples (PBS, Fc, DHA, Gefi, GSSF NPs, DHA@GSSF and CM-DHA@GSSF as 7 group, at an equivalent dose DHA (3.06 mg/kg) and GSSF (16.94 mg/kg) for each mouse) every 2 d for five times. The noninvasive bioluminescence imaging system by Caliper IVIS Spectrum was used to monitor the tumor growth at Day −1, 10 and 20. The mice were euthanized to collect their lung tissues for ex vivo imaging, fixed and H&E staining analysis after 21-d treatment. Additionally, the survival rates of every group were also calculated until Day 40.

3.   Results and discussion

3.1.   Preparation and characterization of CM-DHA@GSSF

The small molecular prodrug GSSF's synthesis route was depicted in Fig. S1, which was synthesized by esterification and amidation reaction with ferrocenecarboxylic acid (Fc), 2,2′-dithiodiethanol, triphosgene and gefitinib, and it was characterized via ^{1}H NMR, HR-MS and ^{13}C NMR (Fig. S2-S5). As shown in Fig. 1A, the biomimetic nano-prodrug CM-DHA@GSSF was composed of DHA@GSSF and A549 cell membrane, which prepared by two-step method. Firstly, small molecular GSSF was self-assembled into nanoparticle DHA@GSSF via the nanoprecipitation method by the addition of DHA into aqueous solution. The absorbance spectrum of GSSF, DHA, Fc, Gefi was shown in Fig. 1B, the spectrum of GSSF overlapped with Fc and Gefi indicating that the GSSF was successfully synthesized. Besides, the small molecular
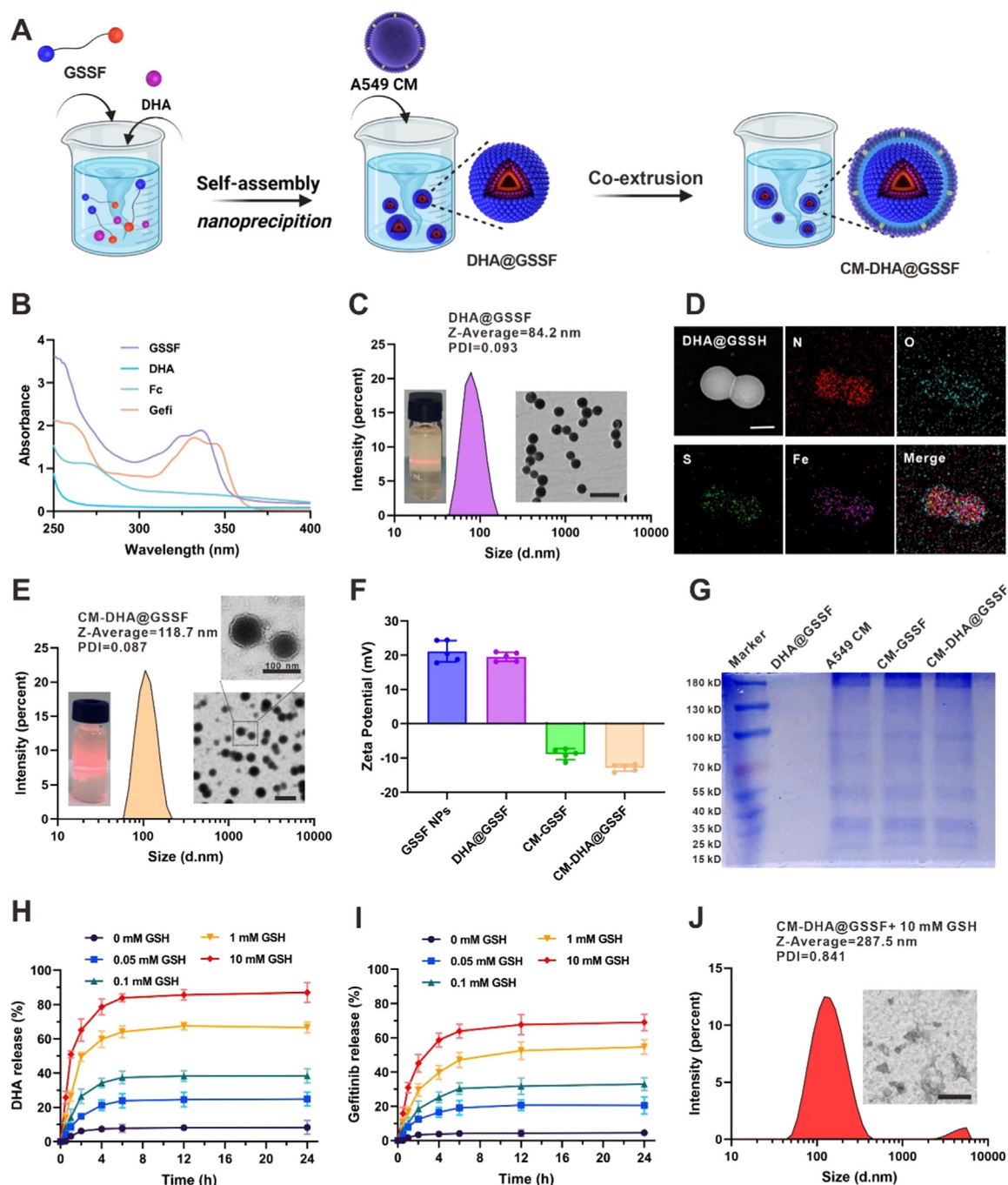
Fig. 1 – The process of fabrication and characterization of CM-DHA@GSSF. (A) Preparation of CM-DHA@GSSF. (B) UV–Vis spectrum of GSSF, DHA, Fc and Gefi. (C) Tyndall effect's photo, size distribution and TEM image of DHA@GSSF, Scale bar: 200 nm. (D) HAADF-STEM of DHA@GSSF. Scale bar: 50 nm. (E) Tyndall effect's photo, size distribution and TEM image of CM-DHA@GSSF, Scale bar: 200 nm. (F) Zeta potential of GSSF NPs, DHA@GSSF, CM-GSSF and CM-DHA@GSSF. (G) SDS-PAGE analysis and staining for DHA@GSSF, A549 CM, CM-GSSF and CM-DHA@GSSF. (H-I) DHA and Gefi release behavior from CM-DHA@GSSF with different GSH concentrations in PBS buffer (pH 7.4) at 37 °C for 24 h. (J) DLS analysis and TEM image of CM-DHA@GSSF after release, Scale bar: 200 nm.

GSSF could change into nanoparticles through disulfide-mediated self-assembly behavior in an aqueous solution, and the particle size and morphology of GSSF NPs were shown in supporting information (Fig. S6), which could form stable and regular nanoparticle. To confirm the drug loading ability of GSSF NPs by its good self-assembly behavior, the dynamic light scattering (DLS) was used to determine the hydromechanical diameter of DHA@GSSF by around 84.2 nm with distributed narrowly (PDI = 0.093), and TEM showed the morphology of the particles was well-shaped spherical

(Fig. 1C). Meanwhile, we also measured the elemental distribution of DHA@GSSF, as shown in Fig. 1D, the O, S or N elements were well overlapped with Fe elements, indicating the successful preparation of DHA@GSSF. Secondly, the A549 cell membrane was coated on the surface of DHA@GSSF to construct the biomimetic nano-prodrug CM-DHA@GSSF. After coating the cell membrane, the hydromechanical diameter of DHA@GSSF increased about 35 nm to 118.7 nm, and its distribution and morphology were more structured (PDI = 0.087), which displayed a clear image of two-layer spherical structure, indicating that the cell membrane was well coated (Fig. 1E). Moreover, the zeta potential clearly revealed that the coating of A549 cell membrane changed the potential from positive to negative significantly due to the electronegativity of cell membrane (Fig. 1F). In addition, we also performed an SDS-PAGE experiment to further confirm successful cell membrane coating of the nanoparticle. In Fig. 1G, no obvious protein bands were observed on DHA@GSSF, while the protein bands of control and CM-DHA@GSSF were nearly identical to those found on A549 cell membranes after coating.

To further investigate the drug release behaviors of CM-DHA@GSSF, we incubated CM-DHA@GSSF with different concentrations of GSH and recorded the release ratio of DHA, Gefi and Fc. As shown in Fig. 1H, 1I and S7, the release ratios of DHA, Gefi and Fc were raised by the increasement of incubation time and GSH level. Moreover, the TEM and DLS of CM-DHA@GSSF after releasement were also performed in Fig. 1J, the diameter and PDI were grown remarkably, and the image of TEM was changed to be more amorphous morphology. Besides, we also investigated the stability of CM-DHA@GSSF in PBS buffer, and there was no obvious change in hydrodynamic size detected by DLS during 7 d (Fig. S8), indicating CM-DHA@GSSF could be stored for a long time. These collective results suggested that our nano-prodrug exhibited good release behavior in TME with high GSH level and was stable under physiological condition.

3.2. Intracellular ferroptosis efficacy

Except for the releasing DHA and Gefi in response to high levels' GSH, CM-DHA@GSSF also could release Fc simultaneously in acid TME, leading to the ·OH generation from Fenton reaction and inducing ferroptosis. To explore the phenomenon, we first conducted a study to investigate the ·OH generation of various formulations using MB degradation assay under a physiological condition. As shown in Fig. 2A, the PBS, Gefi and free DHA demonstrated negligible MB degradation in the presence of 1 mM H_2O_2, while Fc without modification exhibited outstanding ability in MB degradation. As presumed, the nanoparticles that contained Fc molecule (GSSF NPs, DHA@GSSF, and CM-DHA@GSSF) also exhibited remarkable MB degradation capability, indicating the Fc of nanoparticles could generate ·OH via Fenton reaction to degrade MB. To further investigate the ·OH production of CM-DHA@GSSF under physiological conditions and TME, MB degradation assays were also performed under various pH conditions (such as 7.4, 6.8 and 5.5). As shown in Fig. S9A, the degradation of MB raised by the decrease of pH value, indicating that acid environment served as an important role

for the ·OH generation of CM-DHA@GSSF. Moreover, along with the degradation of MB, a noticeable fading of the MB solution's color could be observed with the increasing acid environment, which is nearly bleached under pH 5.5 (Fig. S9B), further proved that an acid environment can facilitate our nano-prodrug to enhance the production of ·OH.

Inspired by the distinguishing feature of our nano-prodrugs in the production of ·OH, we further investigated its ferroptosis efficacy in several cancer cell lines (A549, HepG2, and HeLa) and normal cell lines (LO2 and 293T). We used DCFH-DA, a commercial ROS probe, to visualize the ROS production of CM-DHA@GSSF through fluorescent imaging approach in the various cell lines. As shown in Fig. S10, all cancer cell lines exhibited obvious intracellular green fluorescence intensity, while normal cell lines exhibited imperceptible intracellular fluorescence oppositely. This result revealed that CM-DHA@GSSF had highly capability for producing high ·OH level in cancer cell lines. To investigate ROS generation in A549 cells of different formulations, as shown in Fig. 2B, the weak intracellular green fluorescence signal was displayed in free Fc group due to poor cell uptake by strong hydrophobicity of Fc. Moreover, it was also no obvious intracellular fluorescence signal was observed in the groups of PBS, DHA or Gefi. On the other hand, the nano-formulations groups with Fc component (GSSF NPs, DHA@GSSF and CM-DHA@GSSF) exhibited strong intracellular green fluorescence, and it was worth noting that the nano-formulations that contained DHA (DHA@GSSF and CM-DHA@GSSF) shows more significant fluorescent signal than nano-formulations without DHA (GSSF NPs). These observed differences proved that the nano-formulations could effectively enhance the cellular uptake of Fc into A549 cells, leading to a substantial increase in the production of ·OH, and more importantly, it indicated that DHA as ferroptosis resistance inhibitors could promote ·OH production significantly. In addition, the intracellular green fluorescence of CM-DHA@GSSF in A549 cells was much stronger than that of DHA@GSSF, which was mainly because the coating of CM-DHA@GSSF originated from A549 cells that endowing it with prominent homologous targeting ability.

Solid evidence had confirmed that DHA could decline the GPX4 expression level in ferroptosis resistance process and thus reduce GSH level [27,29,30]. Therefore, we evaluated the intracellular GSH and GPX4 protein expression levels after incubated with different formulations. As shown in Fig. 2C, the intracellular GSH concentrations decreased visibly, meanwhile the nano-formulations that contained DHA exhibited more significant decrease than GSSF NPs (without DHA). On the other hand, the intracellular GSH levels of other groups showed slight differences with the control group, demonstrating that DHA could be release from CM-DHA@GSSF in A549 cells and thus suppress the GSH generation. In order to further explore the nano-prodrugs could serve as a potential GPX4 inhibitor for regulating ferroptosis resistance, we performed a western blot assay to assess the GPX4 protein expression levels in A549 cells treated with different formulations. In Fig. 2D, a significant decrease of the GPX4 expression could be observed upon treatment with DHA, DHA@GSSF, and CM-DHA@GSSF, while there was no significant change in Fc, Gefi, or GSSF groups.
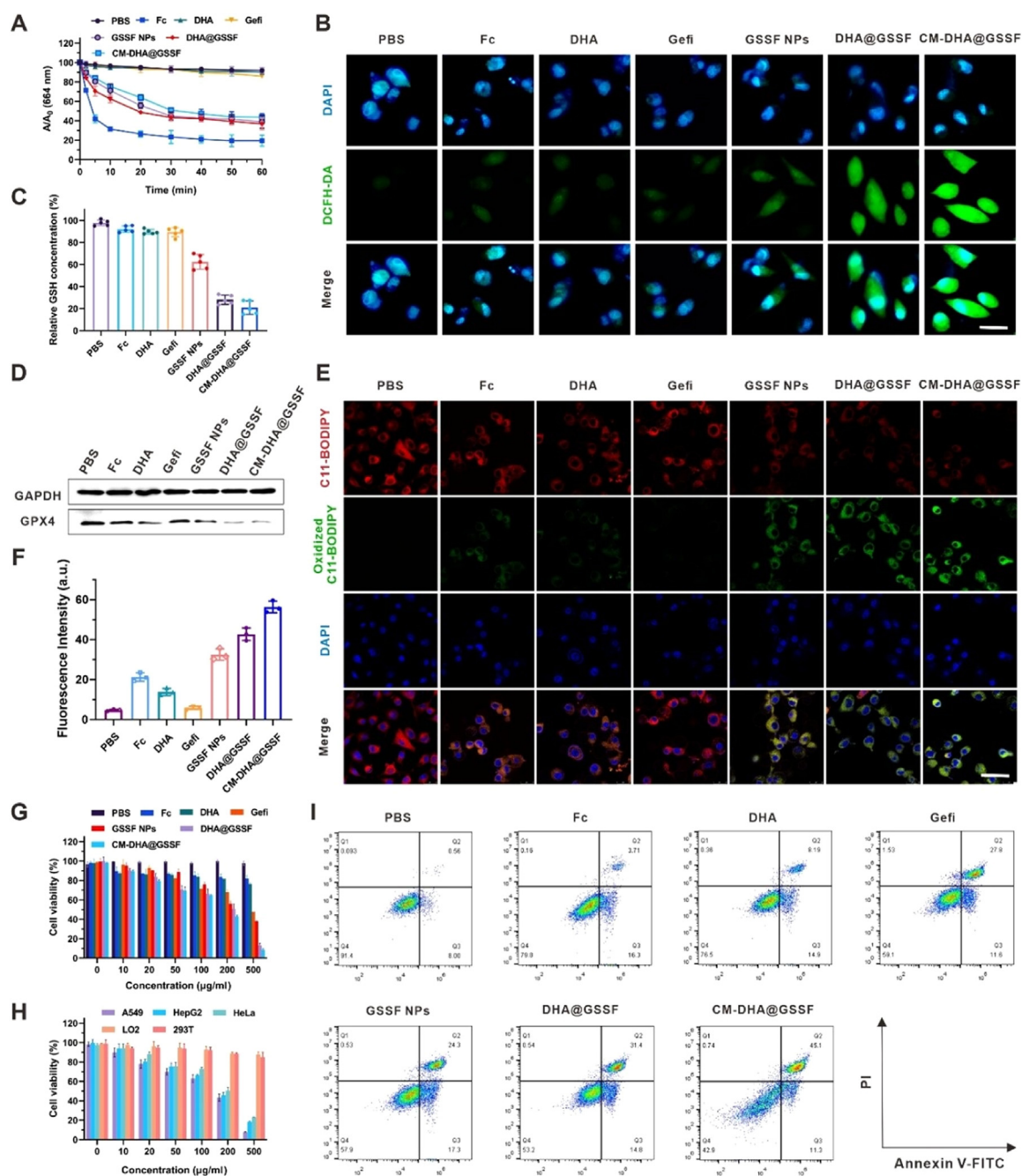
Fig. 2 – The ferroptosis efficacy and cytotoxicity analysis for nano-prodrug *in vitro*. (A) Degradation of MB upon treated with various formulations (PBS, Fc, DHA, Gefi, GSSF NPs, DHA@GSSF, CM-DHA@GSSF) under 1 mM H_2O_2 solution. (B) Fluorescence images of ROS generation after treated with formulations (the ROS probe DCFH-DA shows green fluorescence, and the DAPI serves as cell nucleus indicator and shows blue fluorescence), Scale bar: 25 μm. (C) Relatively GSH levels of A549 cells after various treatments. (D) Western blot results for the GPX4 and GAPDH (control group) expression levels of A549 cells after treated with different formulations. (E) CLSM images of C11-BODIPY-stained A549 cells after treatment with different formulations, Scale bar: 50 μm. (F) Quantitative analysis of green fluorescence intensity of oxidized C11-BODIPY in E. (G) Cell viability of A549 cells treated with different formulations for 48 h. (H) Cell viability of cancer cell group (A549, HepG2, and HeLa) and normal cell group (LO2 and 293T) with CM-DHA@GSSF for 48 h. (I) Flow cytometry analysis results (Annexin V-FITC and PI staining) of A549 cells after treatment with different formulations for 24 h.

These results suggested that the loading DHA into nano-prodrugs could remarkably eliminate the GSH level and inhibit GPX4 expression and thus promote the ferroptosis. As an important marker of ferroptosis, the intracellular LPOs accumulation can induce ferroptosis. To evaluate LPOs level in cancer cells, we used C11-BODIPY as the LPOs probe that could accumulate on the cell membrane and the fluorescence changes from red to green after oxidization. In Fig. 2E, an obvious green fluorescence could be observed after incubation with nano-formulations, and the weakest red fluorescence and the strongest green fluorescence were displayed in CM-DHA@GSSF, suggesting the large amount of LPOs from our nano-prodrug. Furthermore, a similar result was observed by the quantitative analysis results of Fig. 2F. These results are in accordance with the studies of ROS production and demonstrated that CM-DHA@GSSF could generate LPOs and induce ferroptosis in cancer cells.

3.3. In vitro cytotoxicity

To verify the synergistic effect of combined DHA with GSSF, the cell viability of these two drugs at different ratios by CCK8 assay. As shown in Fig. S11, A549 cells were incubated with DHA (alone), GSSF (alone) or DHA/GSSF (different ratios), and there was poor cytotoxicity in DHA (alone) even at high concentrations, while GSSF (alone) exhibited moderate cytotoxicity. Compared with GSSF alone, the combination of GSSF and DHA displayed significantly decreased viability with increasing the concentration of DHA, indicating the good synergistic effect of these two drugs.

To evaluate the in vitro therapeutic performance of nano-prodrugs by the ferroptosis-combined chemotherapy, we first conducted a Live/Dead cell staining assay. As depicted in Fig. S12, A549 cells incubated with CM-DHA@GSSF showed the most number of dead cells (red fluorescence), declaring CM-DHA@GSSF displayed high cytotoxicity. As a control, free Fc and DHA groups exhibited low toxicity and Gefi group exhibited mild cytotoxicity. Furthermore, we proceeded to carry out a CCK8 assay for assessing the cytotoxicity of nano-prodrugs. In Fig. 2G, free Fc and DHA exhibited low cytotoxicity only at high concentrations. Meanwhile, Gefi and nano-formulations showed rather stronger cytotoxicity than that of Fc and DHA, and CM-DHA@GSSF exhibited the strongest cytotoxicity at the same concentration, indicating that the combinational effect induced the high cytotoxicity of A549 cells. Considering the side-effect of CM-DHA@GSSF applied in vivo on normal cells and tissue, a CCK8 assay toward normal cells and cancer cells was carried out. As shown in Fig. 2H, CM-DHA@GSSF showed little cytotoxicity in normal cell lines (LO2 and 293T) while strong cytotoxicity in cancer cell lines (A549, HepG2 and HeLa), which was due to the inactivation of CM-DHA@GSSF under normal physiological conditions and thus reducing side-effect of CM-DHA@GSSF. Since we used Gefi as a chemotherapeutic against tumor cells, a flow cytometry experiment was also carried out to investigate its performance in inducing A549 cell apoptosis. As shown in Fig. 2I, the formulations (Gefi, GSSF NPs, DHA@GSSF and CM-DHA@GSSF) which contained Gefi component showed appreciable apoptosis toxicity toward A549 cells with apoptosis rates (Q2+Q3) of 39.4%, 41.6%, 46.2%

and 56.4%, while the other group showed little apoptosis rates toward A549 cells.

3.4. The drug release behavior and drug distribution of CM-ICG@GSSF in vivo

We first evaluated the hemocompatibility of different formulations via hemolysis assay. As shown in Fig. S13, the hemolysis rate of CM-DHA@GSSF (1.01%) was lower than the other nano-prodrugs, indicating that the cell membrane coated on nano-prodrug could improve the hemocompatibility that was beneficial for prolonging the blood circulations. Before further applications of the biomimetic nano-prodrug CM-DHA@GSSF in vivo, we took an interest in its pharmacokinetic properties in vivo. The pharmacokinetic profiles were assessed by detecting the DHA concentration in plasma after intravenously injected with different self-assembled nano-prodrugs formulations. As shown in Fig. S14, the blood circulating half-life of CM-DHA@GSSF was measured to be 4.52 ± 0.56 h, which is longer than the free DHA (1.27 ± 0.11 h), indicating that the self-assembled nano-prodrugs could prolong the half-life of the drug. Since the A549 cell membrane of CM-DHA@GSSF could give it prominent homologous targeting ability to cancer cells, we chose the DHA@GSSF (without cell membrane) as a control group and changed the parent drug into ICG (indocyanine Green, a commercial fluorescent NIR dye) to investigate the release and distribution of loading drug in tumor-bearing mice. First, we established an A549-subcutaneous xenograft mice model, following intravenously injected the various formulations (ICG, ICG@GSSF, and CM-ICG@GSSF). In Fig. 3A, the fluorescent signal of CM-ICG@GSSF group in tumor region was increased with the prolong of time and reached the maximum at 24 h. The strong fluorescent signal at tumor region was still observed after 48 h. As a control, ICG@GSSF exhibited observable fluorescent signal in the tumor site owing to its EPR effect but rather weaker than CM-ICG@GSSF, and the free ICG group showed no obvious fluorescent signal in the tumor site. Moreover, both ICG-contained group exhibited strong signal at liver area suggesting its metabolism path was liver related. To further investigate drug accumulations, the mice were sacrificed after injection for 48 h, and collected their tumors (T) and main organs (heart (H), liver (Li), spleen (Sp), lung (Lu), and kidney (Ki)) for fluorescent imaging. As shown in Fig. 3B and 3C, both fluorescent image and its corresponding intensity showed the group of CM-ICG@GSSF owning the strongest fluorescent signal, and all ICG-contained groups showed residual signal at liver and kidney indicating its metabolism path was liver and kidney related.

3.5. In vivo tumor inhibition of A549-subcutaneous xenograft model

Inspired by good in vitro therapeutic effect and tumor accumulation of our nano-prodrug, we confidently applied CM-DHA@GSSF in tumor inhibition of A549-subcutaneous xenograft model. The A549 tumor-bearing mice were (tumor volume: about 100 mm^3) randomly divided into 7 groups and then intravenously injected with the various formulations
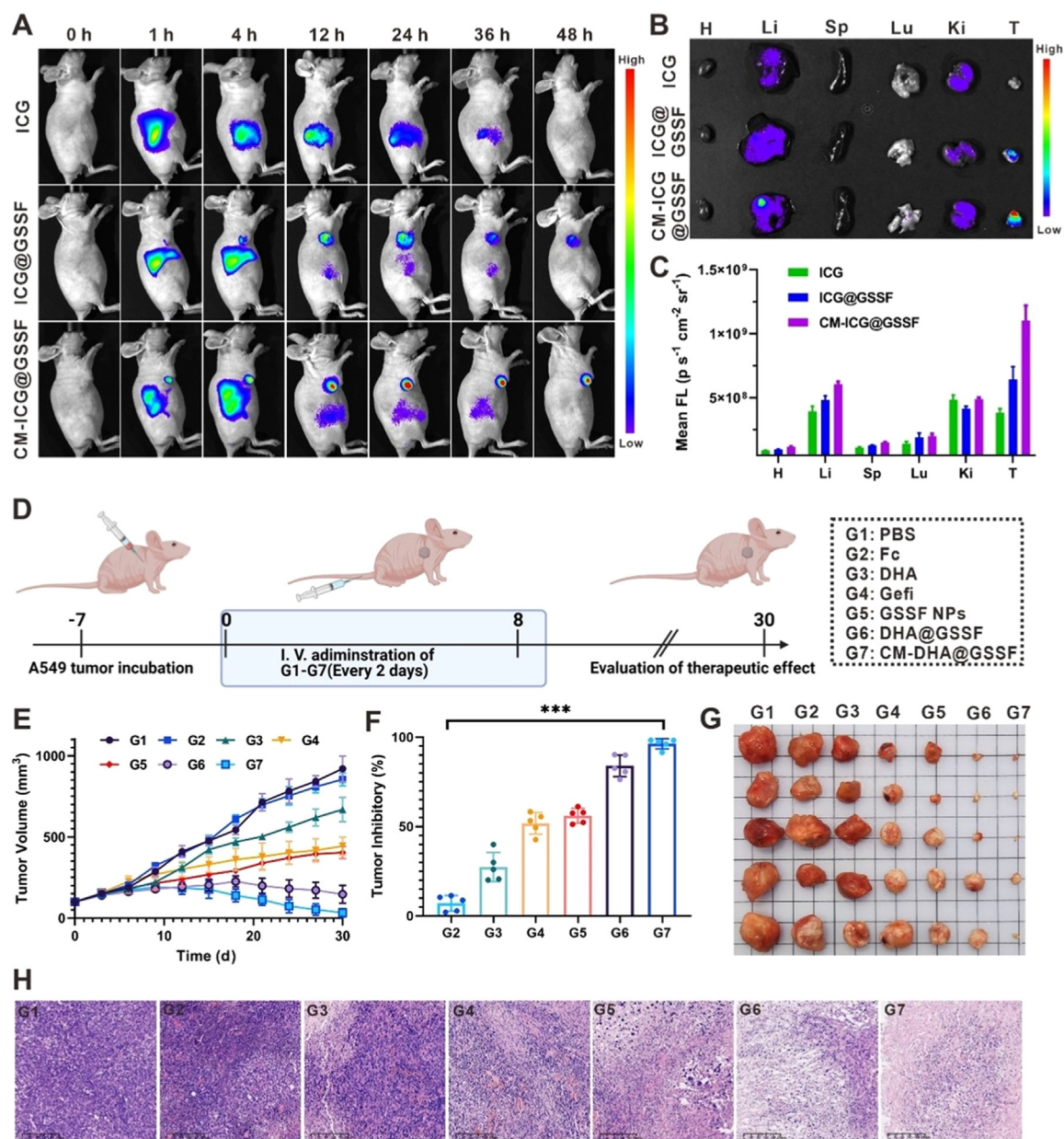
Fig. 3 – The drug distribution of CM-ICG@GSSF *in vivo* and tumor inhibition evaluation of A549-subcutaneous xenograft model. (A) *In vivo* fluorescence images of A549 tumor-bearing mice at different time after intravenous injection ICG, ICG@GSSF, and CM-ICG@GSSF. (B) *Ex vivo* fluorescence images of the dissected tumors and main organs from the mice at 48 h post-injection. (C) Mean fluorescent intensity corresponding to Fig. 3B. (D) Schematic illustration of the therapeutic process for the A549 tumor-bearing mice, the mice were treated with G1-G7(PBS, Fc, DHA, Gefi, GSSF NPs, DHA@GSSF, and CM-DHA@GSSF) via intravenously injection for 5 times, every 2 d and evaluated until Day 30 (*n* = 5). (E) Tumor volume change curves of various treatment groups during the period of treatments. (F) Tumor inhibitory of various treatment groups after treatments. The P-values (***P<0.001) were determined using two-sided Student's t-test. (G) Photograph of anatomical tumors after treatments. (H) H&E staining of tumor from different treatment groups after treatments.

(PBS, Fc, DHA, Gefi, GSSF NPs, CM-DHA@GSSF, and CM-DHA@GSSF, G1-G7, every 2 d, 5 times) (Fig. 3D). In Fig. 3E, tumor growth was recorded during the treatment process, which found the rapid increase in G2 and G3 owing to their poor therapeutic effect. The tumor growth of G4 was relatively inhibited comparing with the control group (G1), but Gefi did not play up to its standard as a classical anti-tumor

drug mainly owing to its poor tumor targeting ability and chemoresistance. On the opposite, nano-formulations (G5-G7) exhibited rather more significant inhibition of tumor growth than any other groups. Moreover, G7 showed the most efficient tumor inhibition whose tumor volume was nearly disappeared after 30-d treatment, which was attributed to its homologous targeting ability and satisfactory combinational
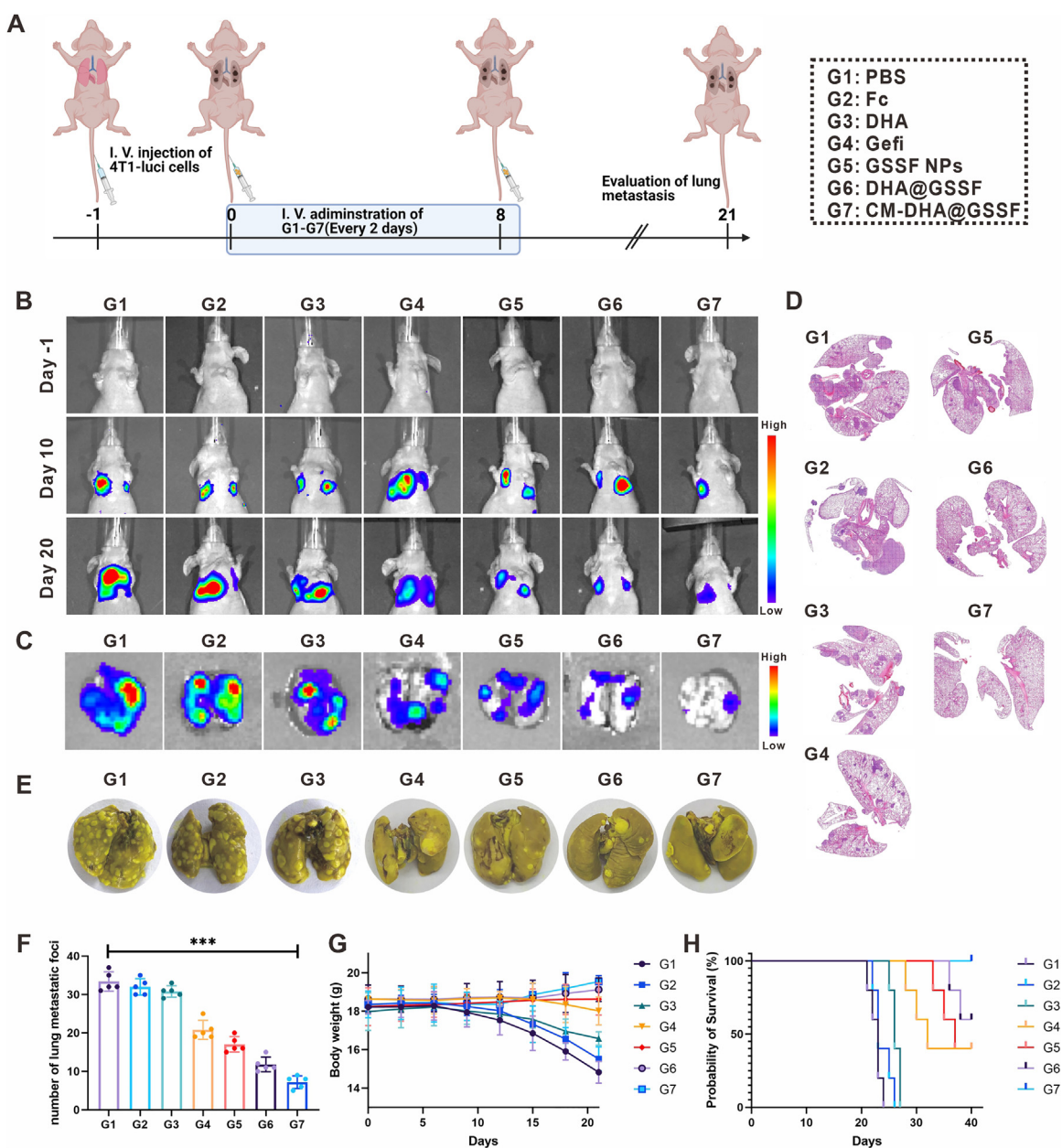
Fig. 4 – Antitumor efficacy on A549-luci lung metastasis model. (A) Schematic illustration of the treatment process of A549-luci lung metastasis, and the mice of G1-G7 were administered with different formulations (PBS, Fc, DHA, Gefi, GSSF NPs, DHA@GSSF, and CM-DHA@GSSF) for 5 times, every 2 d and evaluated until Day 21. **(B)** Representative bioluminescence images of the mice of A549-luci lung metastasis *in vivo*. **(C)** Representative bioluminescence images of lung metastatic nodules after treatments. **(D)** H&E staining analysis of lung sections after treatments. **(E)** Representative photographs of stained lung tissues (Bouin's Fluid) after treatments. **(F)** Calculations of lung metastatic nodules for G1-G7 at the end of treatments. The p-values (***P<0.001) were determined using two-sided Student's t-test. **(G)** The body weight changes of the mice treated with G1-G7 during treatment. **(H)** The profiles of survival rates for the mice treated with G1-G7 within 40 d.

effect. The tumor inhibition rate was also evaluated in Fig. 3F, G7 exhibited good tumor suppression effect. The mice of G1-G7 groups were euthanized and dissected to obtain their tumor tissues after 30-d treatment, and the photos of tumors were exhibited in Fig. 3G, in which G7 were nearly disappeared demonstrating outstanding curative effect of CM-DHA@GSSF. We also analyzed the GPX4 protein expression levels of the tumor tissues in A549-subcutaneous xenograft

model treated with different formulations. As shown in Fig. S15, the GPX4 expression in the group of CM-DHA@GSSF decreased most compared with the control group, suggesting the enhancement of ferroptosis therapeutic effect. Moreover, the H&E staining assays of G1-G7 groups' tumor sections were depicted in Fig. 3H, the nano-formulation (G5-G7) exhibited more histological damage than G2-G4 compared to the control group, and G7 showed the most obvious and strongest

histological damage. All these results above revealed that CM-DHA@GSSF possessed remarkable tumor inhibition of A549-subcutaneous xenograft model.

Furthermore, we assessed the biosafety of our nano-prodrug. As shown in Fig. S16, we tracked the body weight of G1-G7 from Day 0 to Day 30 firstly, and all groups increased steadily at the early treatment stage (Day 0 to Day 15), but the body weight of G3 and G4 dropped obviously from Day 15 to Day 30 mainly because its systemic toxicity of free DHA and Gefi. The other groups showed insignificant differences between the control group indicating well safety. Moreover, we also investigated the survival rate of various groups, as shown in Fig. S17, the G7 group's survival rate was obviously higher than any other groups proving evidence for its high biosafety. Finally, we carried out H&E staining analysis assay for the main organs from the mice treated with G1-G7 to further evaluate the biosafety of each formulation (Fig. S18), and it was clear that there was negligible histological aberration in all groups. All above results reliably confirmed the well biosafety of CM-DHA@GSSF *in vivo*.

3.6.   *Antitumor efficacy on A549-luci lung metastasis model*

Tumor metastasis is one of the major obstacles for the failure in antitumor treatment, the inhibition of tumor metastasis is a critical factor in evaluating the availability and effectiveness of antitumor drugs. Therefore, to evaluate the anti-metastasis potential of our nano-prodrugs by intravenously injecting A549-luci cells, we proceeded to establish a lung metastasis model. As shown in Fig. 4A, after one day, the different formulations (G1-G7: PBS, Fc, DHA, Gefi, GSSF NPs, DHA@GSSF, and CM-DHA@GSSF) were injected into tail vein (5 times, every 2 d). The bioluminescence images of the mice treated with G1-G7 at pre-set time (Day −1, 10 and 20) were shown in Fig. 4B, G7 showed the poor bioluminescence signal at lung area in both mid and later-term treatment, suggesting that CM-DHA@GSSF was well capable of inhibiting tumor metastasis, and the bioluminescence images of anatomical lung tissue after 20-d treatment shown in Fig. 4C were also confirmed that. The H&E staining analysis of lung tissue sections were further confirmed the superior antitumor metastasis ability of CM-DHA@GSSF (Fig. 4D). For further evaluation of tumor metastasis in each group more visually and accurately, we took photographs of stained lung tissue from different formulations at the end of treatment. As shown in Fig. 4E, the metastatic nodules (light yellow spot) on the surface at lungs of G5-G7 were observed rather less than G1-G4, and G7 exhibited the lowest number of lung metastatic nodules among all groups (Fig. 4F). For evaluation the biosafety of these formulations against lung metastatic, the body weight and survival rate of the treatment groups were carried out then. As shown in Fig. 4G and 4H, G7 exhibited steady increase of body weight and the highest probability of survival among all groups. All these results strongly proved the strategy that the combination of Fc, Gefi and DHA synergistic effect plus homologous targeting validated the efficacy and biosafety of CM-DHA@GSSF significantly inhibited tumor metastasis *in vivo*.

4.   Conclusion

In summary, we have successfully developed a biomimetic nano-prodrug system based on small molecular self-assembly for the inhibition of tumor growth and metastasis *in vivo*, which was achieved through the co-delivery of gefitinib, Fc and DHA for enhanced ferroptosis-combined chemotherapy. The nano-prodrug was stable under the normal physiological environment and could disassemble in TME by the cleavage of disulfide bond owing to the high GSH level, thus releasing Fc, DHA and gefitinib to perform enhanced ferroptosis-combined chemotherapy. The released DHA could effectively inhibit the ferroptosis resistance for enhanced the ferroptosis of Fc, further improving the therapeutic effect of gefitinib. In tumor-bearing mouse models, our nano-prodrugs had exhibited outstanding tumor suppression and antitumor metastasis capability, and no noticeable side-effects were observed during treatments. The current study innovatively integrates targeted co-delivery strategy and combination therapy way into a small molecular self-assembly nano-prodrug with satisfactory therapeutic efficacy and biosafety, which provides a new reasonably designed modality for ferroptosis-combined chemotherapy.

Conflicts of interest

The authors declare no conflicts of interest.

Acknowledgments

Supplementary materials

Supplementary material associated with this article can be found, in the online version, at doi:10.1016/j.ajps.2023.100844.

REFERENCES

[1] Conrad M, Pratt DA. The chemical basis of ferroptosis. Nat Chem Biol 2019;15(12):1137–47.

[2] Lei G, Zhuang L, Gan BY. Targeting ferroptosis as a vulnerability in cancer. Nat Rev Cancer 2022;22(7):381–96.

[3] Liang C, Zhang XL, Yang MS, Dong XC. Recent progress in ferroptosis inducers for cancer therapy. Adv Mater 2019;31(51):1904197.

[4] Wan XY, Song LQ, Pan W, Zhong H, Li N, Tang B. Tumor-targeted cascade nanoreactor based on metal-organic frameworks for synergistic ferroptosis-starvation anticancer therapy. ACS Nano 2020;14(9):11017–28.

[5] Shi ZZ, Fan ZW, Chen YX, Xie XF, Jiang W, Wang WJ,

et al. Ferroptosis in carcinoma: regulatory mechanisms and new method for cancer therapy. OncoTargets Ther 2019;12:11291–304.

[6] Jiang YY, Zhao XH, Huang JG, Li JC, Upputuri PK, Sun H, et al. Transformable hybrid semiconducting polymer nanozyme for second near-infrared photothermal ferrotherapy. Nat Commun 2020;11(1):1857.

[7] Tang ZM, Zhao PR, Wang H, Liu YY, Bu WB. Biomedicine meets Fenton chemistry. Chem Rev 2021;121(4):1981–2019.

[8] Yang YX, Zuo SY, Li LX, Kuang X, Li JB, Sun BJ, et al. Iron-doxorubicin prodrug loaded liposome nanogenerator programs multimodal ferroptosis for efficient cancer therapy. Asian J Pharm Sci 2021;16(6):784–93.

[9] Liu T, Liu WL, Zhang MK, Yu WY, Gao F, Li CX, et al. Zhang, Ferrous-supply-regeneration nanoengineering for cancer-cell-specific ferroptosis in combination with imaging-guided photodynamic therapy. ACS Nano 2018;12(12):12181–92.

[10] Xu XM, Chen Y, Gui JY, Liu PL, Huang Y, Shao BH, et al. A biomimetic nanodrug self-assembled from small molecules for enhanced ferroptosis therapy. Biomater Sci 2022;10(3):770–80.

[11] Geng HM, Zhong QZ, Li JH, Lin ZX, Cui JW, Caruso F, et al. Metal ion-directed functional metal–phenolic materials. Chem Rev 2022;122(13):11432–73.

[12] Zhou Z, Li XQ, Hu TT, Xue BL, Chen H, Ma LF, et al. Molybdenum-based nanomaterials for photothermal cancer therapy. Adv NanoBiomed Res 2022;2(11):2200065.

[13] Zhang YC, Li LQ, Li YN, Fei Y, Xue CC, Yao XM. An ROS-activatable nanoassembly remodulates tumor cell metabolism for enhanced ferroptosis therapy. Adv Healthc Mater 2022;11(2):2101702.

[14] Wang WJ, Ling YY, Zhong YM, Li ZY, Tan CP, Mao ZW. Ferroptosis-enhanced cancer immunity by a ferrocene-appended iridium (III) diphosphine complex. Angew Chem Int Ed 2022;134(16):e202115247.

[15] Chen Y, Yao Z, Liu PL, Hu QD, Huang Y, Ping L, et al. A self-assembly nano-prodrug for triple-negative breast cancer combined treatment by ferroptosis therapy and chemotherapy. Acta Biomater 2023;159:275–88.

[16] Zhou Z, Wang YL, Peng F, Meng FQ, Zha JJ, Ma L, et al. Intercalation-activated layered MoO_3 nanobelts as biodegradable nanozymes for tumor-specific photo-enhanced catalytic therapy. Angew Chem Int Ed 2022;134(16):e202115939.

[17] Liu J, Kang R, Tang DL. Signaling pathways and defense mechanisms of ferroptosis. FEBS J 2022;289(22):7038–50.

[18] Yang WS, SriRamaratnam R, Welsch ME, Shimada K, Skouta R, Viswanathan VS, et al. Regulation of ferroptotic cancer cell death by GPX4. Cell 2014;156(1–2):317–31.

[19] Li J, Cao F, Yin HL, Huang ZJ, Lin ZT, Mao N, et al. Ferroptosis: past, present and future. Cell Death Dis 2020;11(2):88.

[20] Zhou Z, Wang T, Hu TT, Cheng CH, Yu SL, Li H, et al. Facile synthesis of 2D Al-TCPP MOF nanosheets for efficient sonodynamic cancer therapy. Mater Chem Front 2023;7:1684–93.

[21] Ursini F, Maiorino M. Lipid peroxidation and ferroptosis: the role of GSH and GPx4. Free Radic Biol Med 2020;152:175–85.

[22] von Krusenstiern AN, Robson RN, Qian NX, Qiu BY, Hu FH, Reznik E, et al. Identification of essential sites of lipid peroxidation in ferroptosis. Nat Chem Biol 2023;19:719–30.

[23] Seibt TM, Proneth B, Conrad M. Role of GPX4 in ferroptosis and its pharmacological implication. Free Radi Biol Med 2019;133:144–52.

[24] He YJ, Liu XY, Xing L, Wan X, Chang X, Jiang HL. Fenton reaction-independent ferroptosis therapy via glutathione and iron redox couple sequentially triggered lipid peroxide generator. Biomaterials 2020;241:119911.

[25] Gutman J, Kovacs S, Dorsey G, Stergachis A, Ter Kuile FO. Safety, tolerability, and efficacy of repeated doses of dihydroartemisinin-piperaquine for prevention and treatment of malaria: a systematic review and meta-analysis. Lancet Infect Dis 2017;17(2):184–93.

[26] Li YN, Li MH, Liu L, Xue CC, Fei Y, Wang X, et al. Cell-specific metabolic reprogramming of tumors for bioactivatable ferroptosis therapy. ACS Nano 2022;16(3):3965–84.

[27] Cui Z, Wang HJ, Li S, Qin TT, Shi H, Ma J, et al. Dihydroartemisinin enhances the inhibitory effect of sorafenib on HepG2 cells by inducing ferroptosis and inhibiting energy metabolism. J Pharmacol Sci 2022;148(1):73–85.

[28] Zhang XK, Yang SB, Wang Q, Ye WM, Liu SL, Wang X, et al. Tailored theranostic nanoparticles cause efficient ferroptosis in head and neck squamous cell carcinoma through a reactive oxygen species "butterfly effect". Chem Eng J 2021;423:130083.

[29] Lin RY, Zhang ZH, Chen LF, Zhou YF, Zou P, Feng C, et al. Dihydroartemisinin (DHA) induces ferroptosis and causes cell cycle arrest in head and neck carcinoma cells. Cancer Lett 2016;381(1):165–75.

[30] Wan XY, Zhong H, Pan W, Li YH, Chen YY, Li N, et al. Programmed release of dihydroartemisinin for synergistic cancer therapy using a $CaCO_3$ mineralized metal-organic framework. Angew Chem Int Ed 2019;58(40):14134–9.

[31] Antoszczak M, Müller S, Cañeque T, Colombeau L, Dusetti N, Santofimia-Castaño P, et al. Iron-sensitive prodrugs that trigger active ferroptosis in drug-tolerant pancreatic cancer cells. J Am Chem Soc 2022;144(26):11536–45.

[32] Wang YJ, Liu D, Zheng QC, Zhao Q, Zhang HJ, Ma Y, et al. Disulfide bond bridge insertion turns hydrophobic anticancer prodrugs into self-assembled nanomedicines. Nano Lett 2014;14(10):5577–83.

[33] Karaosmanoglu S, Zhou MJ, Shi BY, Zhang XJ, Williams GR, Chen XF. Carrier-free nanodrugs for safe and effective cancer treatment. J Control Release 2021;329:805–32.

[34] Yang YX, Zuo SY, Zhang JX, Liu T, Li XM, Zhang HT, et al. Prodrug nanoassemblies bridged by mono-/di-/tri-sulfide bonds: exploration is for going further. Nano Today 2022;44:101480.

[35] Li GT, Sun BJ, Li YQ, Luo C, He ZG, Sun J. Small-molecule prodrug nanoassemblies: an emerging nanoplatform for anticancer drug delivery. Small 2021;17(52):2101460.

[36] Sun BJ, Luo C, Yu H, Zhang XB, Chen Q, Yang W, et al. Disulfide bond-driven oxidation-and reduction-responsive prodrug nanoassemblies for cancer therapy. Nano Lett 2018;18(6):3643–50.

[37] Zhang YZ, Cui HG, Zhang RQ, Zhang HB, Huang W. Nanoparticulation of prodrug into medicines for cancer therapy. Adv Sci 2021;8(18):2101454.

[38] Wang YQ, Luo C, Zhou S, Wang XH, Zhang XB, Li SM, et al. Investigating the crucial roles of aliphatic tails in disulfide bond-linked docetaxel prodrug nanoassemblies. Asian J Pharm Sci 2021;16(5):643–52.